Doppler Effect in Flexible and Expandable Light Waveguide and Development of New Fiber-Optic Vibration/Acoustic Sensor

Kazuro Kageyama, Hideaki Murayama, Kiyoshi Uzawa, Isamu Ohsawa, Makoto Kanai, Yoshiaki Akematsu, Keiich Nagata, and Tetsu Ogawa

***Abstract*—New principle and a geometrical arrangement of an optical fiber for a vibration/acoustic measurement are proposed in the present paper. The sensor is based on a new finding that a frequency of light wave transmitted through a bent optical fiber is shifted by vibration at the bent region. The phenomenon can be explained as Doppler's effect in flexible and expandable light waveguide. Several configurations of the sensor have been designed, and very high sensitivity is achieved in the extremely wide frequency range. Principle, sensor configuration and theoretical sensitivity, measurement system, and some experimental consideration are described in the present paper. The sensor sensitivity was examined experimentally in the low and middle frequency range, and the detectability was confirmed experimentally in the frequency range of acoustic emission signals.**

***Index Terms*—Acoustic emission, displacement measurement, Doppler effect, optical fiber transducers, strain measurement, velocity measurements, vibration measurement.**

I. Introduction

A FIBER-OPTIC sensor has following advantages: 1) small diameter and lightweight, 2) flexibility, 3) high strength, 4) heat resistance, 5) immunity to electromagnetic interference, and 6) durability and corrosive resistance. These characteristics are very adequate to real-time health monitoring of structures in their total life cycle. There are many kinds of fiber-optic sensors developed. The achievements and applications are reviewed, for example, in [1]. There are many types of sensor configurations (Giallorenzi *et al.* [2], Bucaro *et al.* [3], Jackson *et al.* [4]), for example linear, loop and coil, and several methods of interferometers, including homodyne (Dandridge *et al.* [5]), heterodyne, synthetic-heterodyne (Cole *et al.* [6]), etc. Fiber-optic sensors have been applied to measurement of pressure (Hocker [7]), acoustic detection (Giallorenzi *et al.* [2], Bucaro and Hickman [8]) and hydrophone (Bucaro *et al.* [9], Jarzynski *et al.* [10]). Fabry–Pérot interferometer (FPI) and fiber Bragg grating (FBG) sensors have been applied to vibration/acoustic measurements [11]–[13].

Recently, the authors have proposed a new principle and geometrical arrangement of the optical fiber for the vibration/acoustic measurement [14], [15]. The sensor is based on a new finding that frequency of light wave transmitted through a bent optical fiber is shifted by vibration at the bent region. The phenomenon can be explained as Doppler's effect in flexible and expandable light waveguide. Several sensor configurations have been proposed, and very high sensitivity has been achieved in the extremely wide frequency band. Principle, sensor configuration and theoretical sensitivity, measurement system, and some experimental consideration are described in the present paper.

Manuscript received August 11, 2004; revised October 31, 2005.

The authors are with the Department of Environmental and Ocean Engineering, School of Engineering, The University of Tokyo, Tokyo 113-8656, Japan (e-mail: kageyama@giso.t.u-tokyo.ac.jp).

Digital Object Identifier 10.1109/JLT.2005.863331

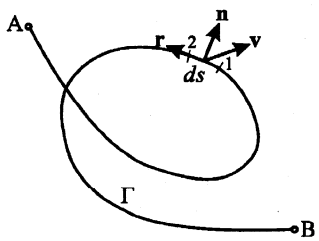

Fig. 1. Flexible and expandable light-waveguide.

II. Doppler Effect in Flexible and Expandable Light Waveguide

Consider the light wave transmission in a media with refractive index n. The light wave with frequency f_0 emitted from a moving point A (light source) is detected at other moving point B (observer). The distance between points A and B changes from L to $L + dL$ during infinitesimal time interval dt. Doppler frequency shift f_D is observed at B by the observer

$$f_D = -\frac{n}{\lambda_0} \cdot \frac{dL}{dt} \tag{1}$$

where λ_0 is the light wavelength in a vacuum, and λ_0/n is the light wavelength in the media.

Next, consider an arbitrary light path (light waveguide), Γ, as shown in Fig. 1. The path is flexible and expandable. It has finite overall length L and two ends, denoted as points A and B, respectively. An incident light from the one end A (light source) is transmitted through the waveguide and detected at the other end B (observer). When the waveguide moves or vibrates, the same equation as (1) is applicable

$$f_D = -\frac{n_{eq}}{\lambda_0} \cdot \frac{dL}{dt} \tag{2}$$

where n_{eq} is the equivalent refractive index of the waveguide and λ_0/n_{eq} is the equivalent length of light wave in the waveguide.

From a geometrical consideration (see detail in Appendix A), dL/dt is given by (3)

$$\frac{dL}{dt} = [\mathbf{v} \bullet \mathbf{t}]_A^B + \int_\Gamma k \cdot \mathbf{v} \bullet \mathbf{n} ds \tag{3}$$

where κ, $\mathbf{v}$, and $\mathbf{n}$ are the curvature, the velocity vector and the unit normal vector of the infinitesimal segment ds, respectively, and $\mathbf{t}$ is the unit direction vector defined at the end points A and B. (See Fig. 1.) The operation $\bullet$ indicates inner product of two vectors.

From (2) and (3), we obtain the following equation:

$$f_D = -\frac{n_{eq}}{\lambda_0}[\mathbf{v} \bullet \mathbf{t}]_A^B - \frac{n_{eq}}{\lambda_0}\int_\Gamma k \cdot \mathbf{v} \bullet \mathbf{n} ds. \tag{4}$$

This equation implies "Doppler effect in flexible and expandable light waveguide." Displacement rate normal to the small segment of the bent optical fiber effects on the frequency shift of the light transmitted through the optical fiber and that the intensity of the frequency shift is proportional to the curvature of the bent fiber. We can detect the local displacement rate at the bent region in the optical fiber. As a feature of sensors, output signal shall return to steady-state value when the external excitation is removed. It requests that the waveguide is elastic, or deformation is reversible.

Behavior of light wave traveling through the media is complex. Exact solution should be obtained by applying special theory of relativity, but the present result gives a sufficient accuracy when motion of light waveguide is much smaller than the light speed.

III. Sensor Configurations and Theoretical Sensitivity

A. Circular Loop

In the case of a circular loop sensor, the sensitivity of strain rate can be evaluated by integrating (4) on the strain-rate field. For simplicity, the uniform strain-rate field, $\dot{\varepsilon}_x, \dot{\varepsilon}_y$ and $\dot{\gamma}_{xy}$ is assumed on the integration path. The velocity vector and the unit normal vector are given by (5) and (6), respectively, where polar coordinate system is employed, as shown in Fig. 2.

$$\mathbf{v} = R\begin{Bmatrix} \dot{\varepsilon}_x \cos\theta + \frac{1}{2}(\dot{\gamma}_{xy} + \dot{\omega}_{xy})\sin\theta \\ \frac{1}{2}(\dot{\gamma}_{xy} - \dot{\omega}_{xy})\cos\theta + \dot{\varepsilon}_y \sin\theta \end{Bmatrix} \tag{5}$$

$$\mathbf{n} = \begin{Bmatrix} \cos\theta \\ \sin\theta \end{Bmatrix} \tag{6}$$

where $\dot{\omega}_{xy}$ and R are rotation term of distortion and radius of the loop, respectively. Substituting (5) and (6) into (4), the theoretical frequency shift f_D^{th} is obtained

$$f_D^{th} = -\frac{\pi R n_{eq}}{\lambda_0}(\dot{\varepsilon}_x + \dot{\varepsilon}_y) = -\frac{\pi R n_{eq}}{\lambda_0}(\dot{\varepsilon}_1 + \dot{\varepsilon}_2). \tag{7}$$

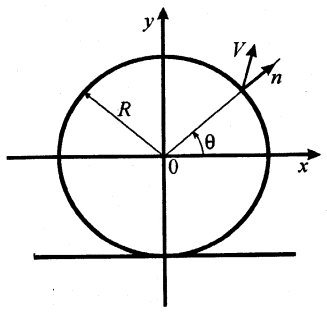

Fig. 2. Circular loop sensor and polar coordinate system.

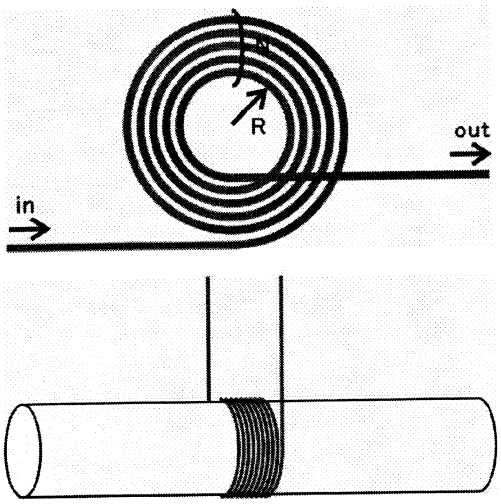

Fig. 3. Examples of circular loop sensors.

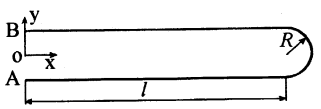

Fig. 4. U-shaped sensor.

The sum of the axial strain rates or the sum of the principal strain rates is converted into the Doppler frequency shift by applying circular loop sensor. Shear strain and rotation have no effect on the frequency shift. In the case of N turns of loop, as shown in Fig. 3, the frequency shift becomes N times larger

$$f_D^{th} = -\frac{N\pi R_{av} n_{eq}}{\lambda_0}(\dot{\varepsilon}_x + \dot{\varepsilon}_y) = -\frac{N\pi R_{av} n_{eq}}{\lambda_0}(\dot{\varepsilon}_1 + \dot{\varepsilon}_2) \tag{8}$$

where $R_{av} = (R_{max} + R_{min})/2$ is the average radius of the loop. The circular loop sensor has no directional sensitivity.

We can control the sensitivity of the sensor by changing the radius and number of turns. The size of the loop is equivalent to a gauge length of the sensor, and it is recommended that the gauge length should be sufficiently smaller than the wavelength of the elastic wave measured.

B. U-Shaped

Frequency change between points A and B along the U-shaped path, as schematically shown in Fig. 4, is considered. On the straight line of the U-shaped path, curvature κ is zero,

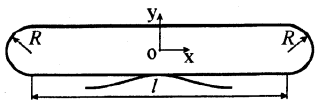

Fig. 5. Elongated circular loop sensor.

and the integral in (4) along the straight lines is zero. On the circular part, the velocity vector and the unit normal vector are given by (9) and (10), respectively

$$\mathbf{v} = \left\{ \begin{array}{l} \dot{\varepsilon}_x \left(R\cos\theta + l\right) + \frac{R}{2}(\dot{\gamma}_{xy} + \dot{\omega}_{xy})\sin\theta \\ \frac{1}{2}(\dot{\gamma}_{xy} - \dot{\omega}_{xy})(R\cos\theta + l) + R\dot{\varepsilon}_y \sin\theta \end{array} \right\}, \quad \left(-\frac{\pi}{2} \le \theta \le \frac{\pi}{2}\right) \tag{9}$$

$$\mathbf{n} = \left\{ \begin{array}{l} \cos\theta \\ \sin\theta \end{array} \right\}. \tag{10}$$

Substituting (9) and (10) into (4), the theoretical frequency shift $f_{\mathrm{D}}^{\mathrm{th}}$ is obtained.

$$f_{\mathrm{D}}^{\mathrm{th}} = -\frac{n_{\mathrm{eq}}}{\lambda_0}\left\{\left(\frac{\pi}{2}R + 2l\right)\dot{\varepsilon}_x + \frac{\pi}{2}R\dot{\varepsilon}_y\right\}. \tag{11}$$

This shape of the sensor has directional sensitivity as a function of l/R. Sensitivity ratio, S_{xy}, of $\dot{\varepsilon}_x$ to $\dot{\varepsilon}_y$ is given by (12)

$$S_{xy} = 1 + \frac{4}{\pi}\cdot\frac{l}{R}. \tag{12}$$

C. Elongated Circular Loop

In the case of an elongated circular loop, as shown Fig. 5, the previous manner of calculation can be applied, and the (13) is obtained

$$f_{\mathrm{D}}^{\mathrm{th}} = -\frac{n_{\mathrm{eq}}}{\lambda_0}\left\{(\pi R + 2l)\dot{\varepsilon}_x + \pi R\dot{\varepsilon}_y\right\}. \tag{13}$$

This shape of the sensor has also directional sensitivity S_{xy}

$$S_{xy} = 1 + \frac{2}{\pi}\cdot\frac{l}{R}. \tag{14}$$

In the case of N turns of loop, the frequency shift becomes N times larger, but the ratio of directional sensitivity is unchanged

$$f_{\mathrm{D}}^{\mathrm{th}} = -\frac{N n_{\mathrm{eq}}}{\lambda_0}\left[(\pi R_{\mathrm{av}} + 2l)\dot{\varepsilon}_x + \pi R_{\mathrm{av}}\dot{\varepsilon}_y\right]. \tag{15}$$

IV. Setup of Measurement System

A laser Doppler velocimeter (LDV) is used to detect the frequency shift. Detection electronics is FM discriminator. Light source is He-Ne laser (output power; 1 mW, wavelength. λ_0: 632.8 nm), and heterodyne interference technique, as shown in Fig. 6, is applied to the measurement in the present paper. An acoustooptical modulator (AOM) changes the frequency of the reference light source from f_0 to $f_0 + f_{\mathrm{M}}$ ($f_{\mathrm{M}} = 80\mathrm{MHz}$) in order to produce beating signals with frequency of $f_{\mathrm{D}} + f_{\mathrm{M}}$.

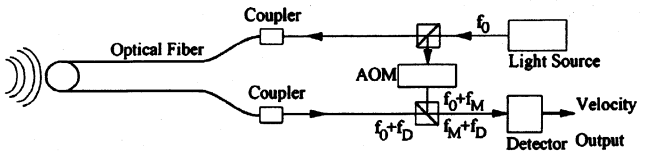

Fig. 6. Setup of measurement system.

The sensitivity of the optical circular fiber sensor (average diameter: 20 mm, number of turn: 10) is calculated theoretically. By applying commercially available performance data of the LDV (Melectro, V1002) [16], the resolution and dynamic range were obtained and listed in Table I. Extremely high resolution less than nanostrain (10^{-10}) is expected in the very wide frequency range from 1 kHz to 1 MHz. Low-frequency vibration of 0.1 Hz is detectable with sufficient sensitivity. The resolution of the newly developed sensor is extremely superior to the other fiber optic sensors, such as FBG. The developed fiber-optic sensor covers the measurement range from conventional strain gauge to AE sensor.

V. Experiments

A. Cyclic Tensile Test

Rectangular aluminum alloy coupon specimen (length: 150 mm, width: 25.0 mm, and thickness: 1.90 mm) was fixed to loading frame by a pair of hydromechanical grips. A circular loop fiber-optic sensor and a conventional strain gauge were bonded on the surfaces of the specimens. Average diameter $2R_{\mathrm{av}}$ of the circular loop is 20 mm, and the number of turns is two. Sinusoidal tensile cyclic load was applied to the specimen by electrohydraulic testing machine. The frequency of the applied load was selected between 2 and 30 Hz.

The polyimide coating and adhesive material and interfacial property between cladding and coating should have effect on the sensitivity. The measured frequency shift f_{D} is expressed as follows:

$$f_{\mathrm{D}} = -K_{\mathrm{a}}\frac{N\pi R_{\mathrm{av}} n_{\mathrm{eq}}}{\lambda_0}(\dot{\varepsilon}_x + \dot{\varepsilon}_y) = -K_{\mathrm{a}}\frac{N\pi R_{\mathrm{av}} n_{\mathrm{eq}}}{\lambda_0}(\dot{\varepsilon}_1 + \dot{\varepsilon}_2) \tag{16}$$

where K_{a} is a calibration coefficient. Measured calibration coefficient value K_{a} is listed in Table II. K_{a} value is almost independent of the frequency and the average value is 0.834. From the theoretical point of view, K_{a} shall be near one but not exceed one. The experimental data well agrees with the theoretical condition.

B. Vibration of Cantilever Beam

Because of extremely wide frequency range of the developed fiber-optic sensor, we need to apply multiple methods to calibrate the sensitivity. In the present paper, conventional electrical resistance strain gauge was used in order to examine the strain amplitude of a vibrating metallic beam plate in the frequency range from 100 to 440 Hz. A single mode optical fiber coated with polyimide polymer was used for a 2-turn loop sensor with average diameter $2R$ of 16.2 mm.

TABLE I
SPECIFICATION OF OPTICAL LOOP FIBER SENSOR (DIAMETER: 20 mm, NUMBER OF TURNS: 10): CALCULATED VALUES

Frequency Range		0.1 Hz - 3 MHz				
Resolution (at Ranges (4))		10 Hz	1 kHz	10 kHz	100 kHz	1 MHz
	Strain Rate (με/s)	0.44			4.4	44
	Strain (με)	0.01	0.0001	0.00001	0.00001	0.00001
Total Dynamic Range (dB)		160			140	120

TABLE II
MEASURED CALIBRATION COEFFICIENT VALUE K_a OF CIRCULAR LOOP SENSOR (DIAMETER: 20 mm, NUMBER OF TURNS: 2): TENSILE TEST

Frequency	1.98	3.04	5.03	7.09	9.98	19.82	30.0	Average
K_a value	0.852	0.846	0.841	0.830	0.831	0.818	0.820	0.834

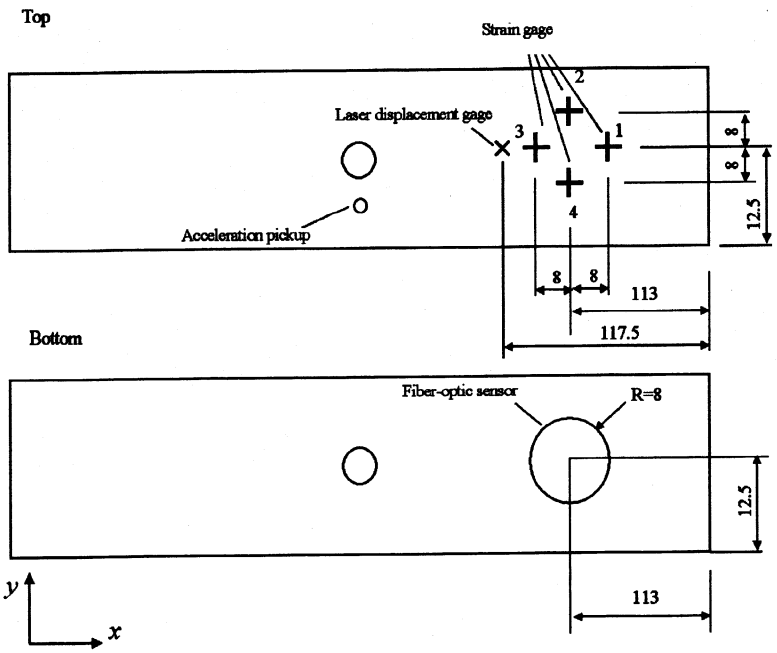

Fig. 7. Vibration beam plate specimen and sensor arrangements.

Configuration of the beam plate specimen and arrangement of sensors are shown in Fig. 7. Four sheets of cross strain gauges are pasted on the same location but opposite surface of the fiber-optic loop sensor. Average values of ε_x and ε_y were obtained from the four sets of the cross strain gauges. Deflection of the beam was measured with a noncontacted laser displacement pickup. The vibrating force was subjected to the center of the plate, and the force was monitored with an accelerometer.

Because of the low sensitivity of the conventional strain gauge, it can measure the strain amplitude with comparable accuracy only at the resonance frequency. The second mode of resonance vibration was used for measurement. The location of the fiber-optic loop sensor and strain gauges were determined from the finite element analysis. In order to change the resonance frequency, thickness of the plate was changed in four steps of 1, 2, 3, and 4 mm, which are related to the resonance frequency of 105, 210, 324, and 438 Hz, respectively.

Examples of the detected vibrations are shown in Fig. 8. Difference of phase between the strain gauge and the fiber-optic sensor is $\pi/2$, it means the fiber-optic sensor detects the strain rate. The amplitude of the sensor output was measured

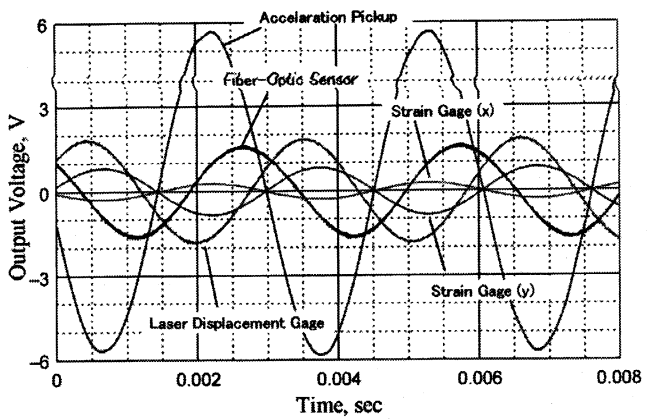

Fig. 8. Examples of detected sensor outputs.

with lock-in amplifier. Calibration coefficient K_a was experimentally determined by comparing the output signal of the fiber-optic sensor and the strain gauges. The result was shown in Fig. 9. K_a is almost independent of the frequency and the average value is 0.84.

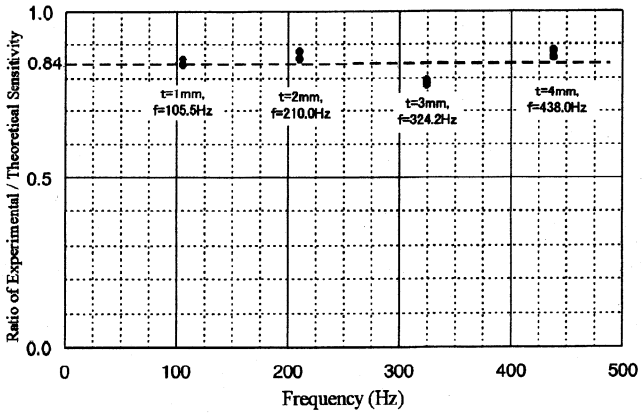

Fig. 9. Calibration coefficient K_a experimentally determined: Cantilever beam test.

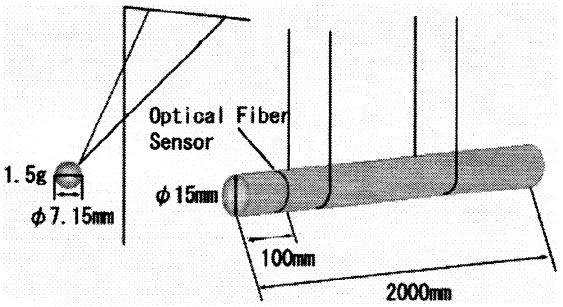

Fig. 10. Impulse force of a small ball to a long bar.

C. Elastic Wave Propagation in a Long Bar Impacted by Collision of Small Ball

In order to examine the dependence of sensitivity on frequency over 500 Hz, elastic wave propagation in a long steel bar, whose end was impacted by collision of a small steel ball, was measured by the fiber-optic sensor. Specimen and test setup are schematically shown in Fig. 10. Diameter and length of the steel bar are 15 mm and 2 m, respectively. Mass and diameter of the steel ball are 1.5 g and 7.15 mm, respectively. Impact velocity of the ball was chosen as 1, 2, and 3 m/s. Optical fiber is wrapped around the steel bar, as shown in Fig. 10, and the velocity V_R in the radial direction was measured. According to (4), there is a linear relation between Doppler frequency shift f_D and radial velocity V_R

$$f_D = -K_a \frac{2N\pi n_{eq}}{\lambda_0} \cdot V_R. \tag{17}$$

Time history of the impact force is calculated from Hertz's dynamic elastic contact theory (See Appendix B). The theoretical time history is used as input of impact force to the end of the elastic bar, and propagation of the elastic wave is calculated with finite element method (see detail in Appendix C). The experimental result of the radial velocity V_R is compared with the numerical one in Fig. 11. Transfer function of the sensor system is obtained by assuming the input and output signals as the numerical and experimental results, respectively. The results of gain and phase of the transfer functions are plotted in Fig. 12(a) and (b), respectively. The sensitivity of the fiber-optic sensor is nearly constant in the frequency range between 10 and 80 kHz.

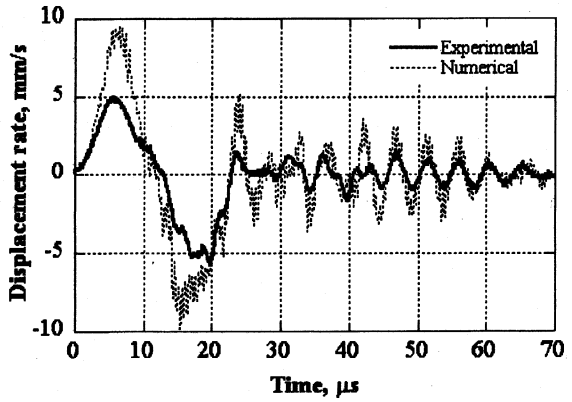

Fig. 11. Time history of displacement rate of elastic wave propagating in a long rod.

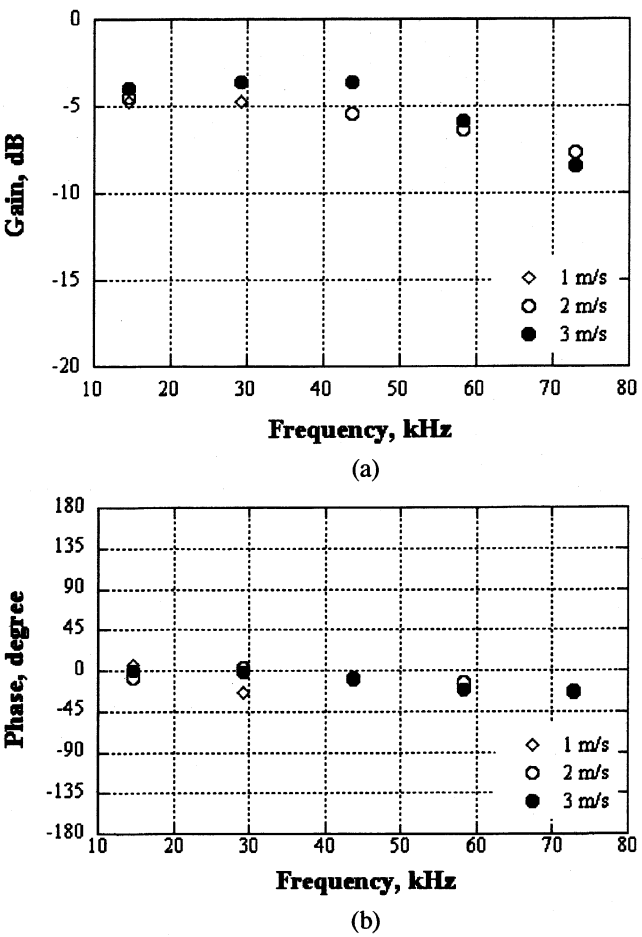

Fig. 12. Frequency characteristics estimated. (a) Gain. (b) Phase.

D. Quasi-AE Wave

Performance test as an AE detector was carried out in the present paper. A PZT vibrator generates quasi-AE waves with main frequency of 150 kHz on a steel plate (800 mm × 800 mm × 3 mm). The quasi-AE waves were detected with

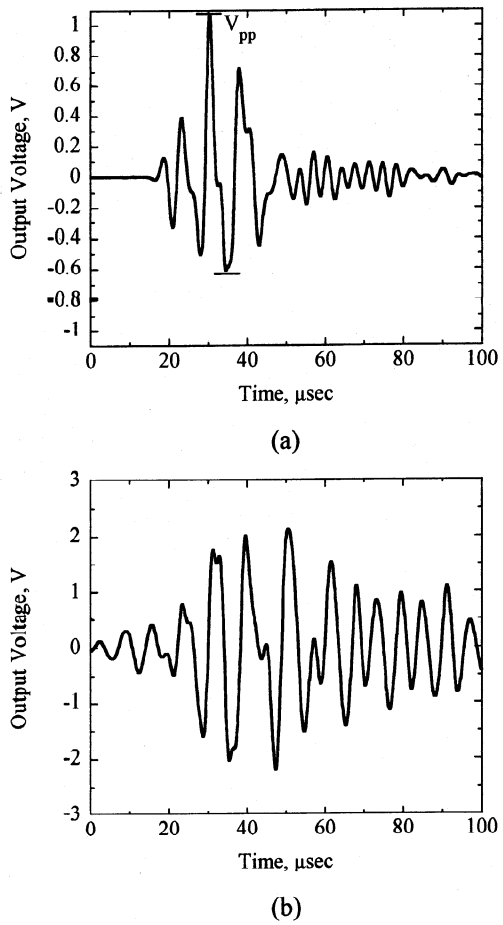

Fig. 13. Quasi-AE waves detected with the fiber-optic sensor and a PZT AE sensor. (a) Fiber-optic sensor with loops of $2R = 10$ mm and $N = 10$. (b) Conventional resonant-type PZT AE sensor.

the developed fiber-optic sensor (circular-shaped) and a conventional PZT resonant-type AE sensor. Fig. 13 shows a result of fiber-optic sensor with loops of $2R = 10$ mm and $N = 10$ [Fig. 13(a)] compared with PZT AE sensor [Fig. 13(b)].

Sensitivity of the new fiber-optic sensor is almost equivalent to the conventional AE sensor. Duration of the fiber-optic sensor is smaller than that of the PZT sensor. Authors think that it shows excellent linear sensitivity of the newly developed optical sensor.

VI. Conclusion

New principle and a geometrical arrangement of optical fiber for vibration/acoustic measurement are proposed in the present paper. The principle of the sensor can be understood as Doppler's effect in flexible and expandable light waveguide. Theoretical strain-rate sensitivity of circular loop, U-shaped, and elongated circular loop sensors have been theoretically obtained. The sensor sensitivity was examined experimentally in the low and middle frequency range, and the detectability was confirmed in the wide frequency range from 1 Hz to 80 kHz, or AE signals. By applying commercially available performance data of LDV, the resolution of the sensor was calculated. Extremely high resolution less than nanostrain (10^{-10}) is expected in the very wide frequency range from 1 kHz to 1 MHz.

Appendix A

Consider the infinitesimal segment ds of an arbitrary path, as shown in Fig. 1. Light wave is transmitted from point 1 to point 2 in the segment. The segment moves at the velocity vector $\mathbf{v}$. Unit direction vector $\mathbf{t}$ and the unit normal vector $\mathbf{n}$ are defined, as shown in Fig. 1. The velocity vector of the fiber motion measured at points 1 and 2 are $\mathbf{v}_1$ and $\mathbf{v}_2$, respectively. Direction change along the infinitesimal segment ds is $d\theta$.

Elongation velocity of the segment ds is given by

$$d\left(\frac{dL}{dt}\right) = (\mathbf{v}_2 \bullet \mathbf{t} - \mathbf{v}_1 \bullet \mathbf{t}) = \mathbf{dv} \bullet \mathbf{t}. \tag{A1}$$

Operation $\bullet$ indicates inner product of two vectors, and the gradient d/ds is given as

$$\frac{d}{ds}\left(\frac{dL}{dt}\right) = \frac{\mathbf{dv}}{ds} \bullet \mathbf{t} = \frac{d}{ds}(\mathbf{v} \bullet \mathbf{t}) - \mathbf{v} \bullet \frac{\mathbf{dt}}{ds}. \tag{A2}$$

Integrating (A2) along the arbitrary path Γ as shown in Fig. 1.

$$\frac{dL}{dt} = [\mathbf{v} \bullet \mathbf{t}]_A^B - \int_\Gamma \mathbf{v} \bullet \frac{\mathbf{dt}}{ds} ds = [\mathbf{v} \bullet \mathbf{t}]_A^B + \int_\Gamma \mathbf{v} \bullet \mathbf{n} d\theta$$
$$= [\mathbf{v} \bullet \mathbf{t}]_A^B + \int_\Gamma \kappa \mathbf{v} \bullet \mathbf{n} ds \tag{A3}$$

where geometrical relations

$$\frac{\mathbf{dt}}{ds} = -\mathbf{n} \bullet d\theta \quad \text{and} \quad d\theta = \kappa ds \tag{A4}$$

are used in (A3).

Appendix B

Let an elastic ball of mass m and radius r strike the end of an infinitely long cylindrical bar with velocity V_0 in longitudinal impact. It is assumed that the ball and the bar have the same material properties. Call $\beta(t)$ the relative displacement of the centers of mass of ball and bar. Newton's law at $x = 0$, at the end of the bar which the ball is impacted, gives the velocity of the impacting ball [17]

$$v = V_0 - \frac{1}{m}\int_0^t F(t)dt. \tag{B1}$$

The Hertzian law of impact gives

$$F = K\beta^{\frac{3}{2}} \tag{B2}$$

$$K = \frac{2}{3}\frac{E}{1-\nu^2} r^{\frac{1}{2}}. \tag{B3}$$

TABLE III
MATERIAL CONSTANT

Density, ρ	Modulus of elasticity, E	Cross-sectional area of the bar, A	Radius of the ball, r	Poisson's ratio, ν
7860 kg/m^3	2.1x10^{+11}N/m^2	0.0001767 m^2	3.58 mm	0.3

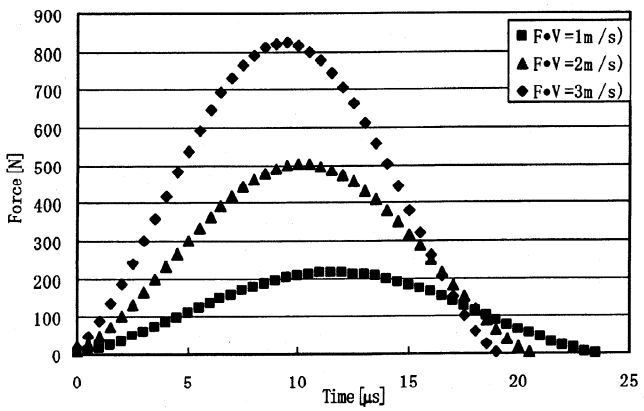

Fig. 14. Calculated force–time relationships.

From (B1) and (B2), the following differential equation in the variable β is obtained

$$\frac{d^2\beta}{dt^2} + \frac{K}{\rho C_0 A}\frac{d\beta^{\frac{3}{2}}}{dt} + \frac{K}{m}\beta^{\frac{3}{2}} = 0 \qquad \text{(B4)}$$

where ρ is the density, $C_0 = (E/\rho)^{1/2}$ the velocity of the stress-wave uniformly distributed across the section of the cylindrical bar, A the cross-sectional area of the bar, E the modulus of elasticity, ν the Poisson's ratio, and F, the force between the ball and the bar. Equation (B4) was solved numerically for the initial conditions; $\beta = 0, v = V_0$ at $t = 0$.

The values in Table III were substituted in (B4). Three different impact velocities were considered: 1, 2, and 3 m/s. By using Mathematica (Wolfram Research) to numerically solve (B4), the change in β were obtained. Substituting the values of β and (B3) in (B2), the time history of impact force F was obtained. The results were shown in Fig. 14.

APPENDIX C

The results of Appendix B were used as mechanical loads in finite element analysis. By using MSC Software Corporation Marc Mentat, finite element model was built and MSC Marc (MSC Software) was used for Finite element analysis. The model was assumed as symmetrical with respect to the central axis of the bar. Fig. 15 is a view showing the models. The model was divided into 20 000 elements ($2000 * 10$). Each element is 1 mm $*$ 0.75 mm. The 4-node axisymmetric quadrilateral element (isoparametric) was used. The boundary condition was free, and the calculated mechanical loads were given as Fig. 14, according to the three different impact velocities' models. The values of material constants in Table III were used.

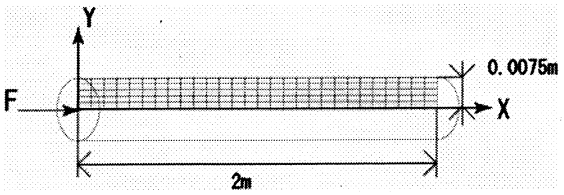

Fig. 15. Finite element model and mesh division.

Newmark-beta operator ($\gamma = 0.5, \beta = 0.25$) was used, and time step was 0.1 μs.

ACKNOWLEDGMENT

The authors thank Prof. K. Hotate, the University of Tokyo, for a fruitful discussion on the principle of the sensor. The authors also thank Y. Machijima, Dr. F. Matsumura, and S. Takahashi, LAZOC, Inc. for technical supports to the new fiber-optic sensing system.

REFERENCES

[1] E. Udd *et al.*, *Fiber Optic Smart Structures*, E. Udd, Ed. New York: Wiley, 1995.
[2] T. G. Giallorenzi, J. A. Bucaro, A. Dandridge, G. H. Sigel, Jr., J. H. Cole, S. C. Rashleigh, and R. G. Priest, "Optical fiber sensor technology," *IEEE J. Quantum Electron.*, vol. QE-18, no. 4, pp. 626–665, Apr. 1982.
[3] J. A. Bucaro, N. Lagakos, J. H. Cole, and T. G. Giallorenzi, "Fiber optic acoustic transduction," *Phys. Acoust.*, vol. XVI, no. 7, pp. 385–457, 1982.
[4] D. A. Jackson, R. Priest, A. Dandridge, and A. B. Tveten, "Elimination of drift in a single-mode optical fiber interferometer using a piezoelectrically stretched coiled fiber," *Appl. Opt.*, vol. 19, no. 17, pp. 2926–2929, Sep. 1980.
[5] A. Dandridge, A. B. Tveten, and T. G. Giallorenzi, "Homodyne demodulation scheme for fiber optic sensors using phase generated carrier," *IEEE J. Quantum Electron.*, vol. QE-18, no. 10, pp. 1647–1653, Oct. 1982.
[6] J. H. Cole, B. A. Danver, and J. A. Bucaro, "Synthetic-heterodyne interferometric demodulation," *IEEE J. Quantum Electron.*, vol. QE-18, no. 4, pp. 694–697, Apr. 1982.
[7] G. B. Hocker, "Fiber-optic sensing of pressure and temperature," *Appl. Opt.*, vol. 18, no. 9, pp. 1445–1448, May 1979.
[8] J. A. Bucaro and T. R. Hickman, "Measurement of sensitivity of optical fibers for acoustic detection," *Appl. Opt.*, vol. 18, no. 6, pp. 938–940, Mar. 1979.
[9] J. A. Bucaro, H. Dardy, and E. F. Carome, "Fiber-optic hydrophone," *J. Acoust. Soc. Amer.*, vol. 62, no. 5, pp. 1302–1304, 1977.
[10] J. Jarzynski, R. Hughes, T. R. Hickman, and A. Bucaro, "Frequency response of interferometric fiber-optic coil hydrophone," *J. Acoust. Soc. Amer.*, vol. 69, no. 6, pp. 1799–1808, 1981.
[11] I. Read, P. Foote, and S. Murray, "Optical fibre acoustic emission sensor for damage detection in carbon fibre composite structures," *Meas. Sci. Technol.*, vol. 13, no. 1, pp. N5–N9, 2002.
[12] I. Perez, H.-L. Cui, and E. Udd, "Acoustic emission detection using fiber Bragg gratings," *Proc. SPIE*, vol. 4328, pp. 209–215, 2001.
[13] G. Thursby, B. Sorazu, D. Bets, W. Staszewski, and B. Culshaw, "Comparison of point and integrated fiber optic technique for ultrasound detection and location of damage," in *Proc. SPIE, Smart Structures and Materials*, 2004, vol. 5384, pp. 287–295.

[14] K. Kageyama, H. Murayama, I. Ohsawa, M. Kanai, T. Motegi, K. Nagata, Y. Machijima, and F. Matsumura, "Development of a new fiber-optic acoustic/vibration sensor: Principle, sensor performance, applicability to health monitoring and characteristics at elevated temperature," in *Proc. Struct. Health Monitoring*, 2003, pp. 1150–1157.
[15] K. Kageyama, H. Murayama, I. Ohsawa, M. Kanai, K. Nagata, Y. Machijima, and F. Matsumura, "Acoustic emission monitoring of a reinforced concrete structure by applying new fiber-optic sensors," *Smart Mater. Struc.*, vol. 14, no. 3, pp. S52–S59, Jun. 2005.
[16] *Technical Report of "VIBRODUCER V1002"*, 2002, Denshigiken Co. Ltd., Kawasaki, Japan.
[17] C. S. Barton, E. G. Volterra, and S. J. Cirton, "On elastic impacts of spheres on long rods," in *Proc. 3rd US Nat. Congr. Appl. Mech.*, 1958, pp. 89–94.

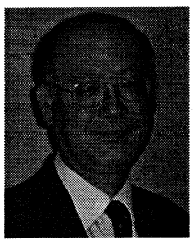

Kazuro Kageyama received the Ph.D. degree in engineering from the University of Tokyo, Tokyo, Japan, in 1981.

During 1981–1988, he was a research official with the Mechanical Engineering Laboratory, Agency of Industrial Science and Technology. He joined the University of Tokyo as an Associate Professor, in 1988, and now is a Professor of the Department of Environmental and Ocean Engineering, School of Engineering, the University of Tokyo.

Dr. Kageyama is a Board Member of The Japan Society for Composite Materials, a Fellow of Japan Society of Mechanical Engineer, and a member of The Society of Naval Architects of Japan, The Society of Materials Science, Japan, Japan Society of Civil Engineering, and Society for the Advancement of Material and Process Engineering (SAMPE).

Hideaki Murayama received the Ph.D. degree in engineering from the University of Tokyo, Japan, in 2001.

He is a Lecturer of the Department of Environmental and Ocean Engineering, School of Engineering, the University of Tokyo.

Dr. Murayama is a member of the Japan Society of Mechanical Engineers, the Society of Naval Architects of Japan, and the Japan Society for Composite Materials.

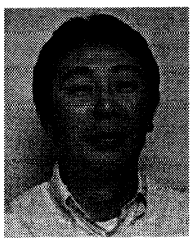

Kiyoshi Uzawa received the M.S. degree in mechanical engineering from Sophia University, Tokyo, Japan, in 1985.

He is a Research Associate with the Department of Environmental and Ocean Engineering, School of Engineering, the University of Tokyo. He was with Honda R&D Ltd., from 1985 to 1991. From 1991 to 2003, he was engaging in the business of designing and constructing advanced composite material products. His current research interests are composite structure design and structural health monitoring using fiber optic sensors.

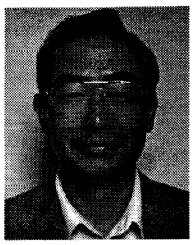

Isamu Ohsawa received the Ph.D. degree in engineering from the University of Tokyo, Tokyo, Japan, in 2001.

He is a Research Associate of the Department of Environmental and Ocean Engineering, School of Engineering, the University of Tokyo, Japan. Specialize in the evaluation of mechanical properties and fracture process of fiber reinforced plastics by means of acoustic emission (AE) technique.

Makoto Kanai received the B.S. degree in composite material engineering, mechanical engineering, and material testing from Tokyo Denki University, Tokyo, Japan, in 1977.

He is a Staff Engineer of the University of Tokyo.

Yoshiaki Akematsu received the Ph.D. degree in mechanical engineering from the University of Tokushima, Tokushima, Japan in 2003.

He is a Postdoctoral Researcher of the Department of Environmental and Ocean Engineering, School of Engineering, the University of Tokyo, Tokyo, Japan.

Dr. Akematsu is a member of the Japan Society for Composite Materials (JSCM).

Keiich Nagata, photograph and biography not available at the time of publication.

Tetsu Ogawa, photograph and biography not available at the time of publication.